SUPPORTING INFORMATION

Tumor Retention of Enzyme-Responsive Pt(II) Drug-Loaded Nanoparticles Imaged by Nanoscale Secondary Ion Mass Spectrometry and Fluorescence Microscopy

Maria T. Proetto, [†,‡] Cassandra E. Callmann, [†,‡] John Cliff, [§] Craig J. Szymanski, [§] Dehong Hu, [§] Stephen B. Howell, [∥] James E. Evans, [§] Galya Orr [§] and Nathan C. Gianneschi *[†,‡]

[†] Department of Chemistry & Biochemistry and [∥] Moores Cancer Center, University of California, San Diego, La Jolla, California 92093, United States

[‡] Department of Chemistry, Department of Materials Science & Engineering, Department of Biomedical Engineering, Northwestern University, Evanston, Illinois 60208, United States

[§] Environmental Molecular Sciences Laboratory (EMSL), Pacific Northwest National Laboratory, Richland, Washington 99354, United States

Contents

(nanocarrier) and $^{195}Pt^-$ (Pt-drug). The correlation was carried out for images from the three different studied conditions: tumor sections from mice treated with ***L*-Pep-Pt-NP**, ***D*-Pep-Pt-NP** and saline solution

Statistical Analysis of NanoSIMS Data

Figure S12. Inside and outside of ^{15}N-rich ROIs selected from HSI NanoSIMS images and inside and outside of ^{31}P-rich ROIs selected on $^{31}P^-$ NanoSIMS ion maps

Table S1. $^{15}N/^{14}N$ and ^{195}Pt counts for ROIs selected inside and outside of ^{15}N-rich areas

Table S2. $^{15}N/^{14}N$ and ^{195}Pt counts for ROIs selected inside and outside of ^{31}P-rich areas

Table S3. Statistical analysis for graphs on Figure 5 of the main text

General Materials and Methods

All reagents were purchased from VWR, Alfa Aesar, or Sigma-Aldrich and used without further purification. Sealed ampules of DMF-d_7 (Cambridge Isotopes) were used without further purification. Modified second generation Grubbs' ruthenium initiator, $(IMesH_2)(C_5H_5N)_2(Cl)_2Ru{=}CHPh$, was prepared as previously described (Sanford *et al. Organometallics*, **2001**, *20*, 5314). Drug, ^{15}N, peptide, and Cy5.5 monomers were synthesized as previously reported (Proetto *et al. ACS Nano,* **2016**, *10*, 4046 and Callmann *et al. Adv Mater* **2015**, *27*, 4611). MMP-12 (catalytic domain) was obtained from Enzo Life Sciences as a solution in 50 mM TRIS, pH 7.5, containing 1 mM calcium chloride, 300 mM sodium chloride, 5 μM zinc chloride, 0.1% Brij-35 and 15% glycerol. HPLC analyses of all products and peptides were performed on a Jupiter 4u Proteo 90A Phenomenex column (150 x 4.60 mm) with a binary gradient, using a Hitachi-Elite LaChrom 2130 pump that was equipped with a Hitachi-Elite LaChrom L-2420 UV-Vis detector. Separation was achieved with a flow rate of 1 mL min^{-1} and the following mobile phase: 0.1% trifluoroacetic acid in H_2O (A) and 0.1% trifluoroacetic acid in ACN (B). Starting with 100% A and 0% B, a linear gradient was run for 30 min to a final solvent mixture of 33% A and 67% B, which was held for 5 min before ramping up to 0% A and 100% B over the course of 2 min and holding at this level for an additional 4 minutes, before ramping back down to 100% A and 0% B, with constant holding at this level for 4 an additional minutes. Mass spectrometry (MS) of all synthesized compounds and peptides was performed at the Molecular Mass Spectrometry Facility (MMSF) in the Department of Chemistry and Biochemistry at the University of California, San Diego. Polymer dispersities and molecular weights were determined by size-exclusion chromatography (Phenomenex Phenogel 5u 10, 1k-75k, 300 x 7.80 mm in series with a Phenomex Phenogel 5u 10, 10K-1000K, 300 x 7.80 mm (0.05 M LiBr in DMF)) using a Shimadzu pump equipped with a multi-angle light scattering detector (DAWN-HELIOS: Wyatt Technology) and a refractive index detector Wyatt Optilab TrEX normalized to a 30,000 MW polystyrene standard. Particle diameters were determined by dynamic light scattering (DLS, D_{DLS}) using a Wyatt Dynapro NanoStar. TEM images were acquired on carbon grids (Ted Pella, INC.) using a FEI Tecnai G2 Sphera at 200 KV. TEM grids were prepared with a 1% uranyl acetate stain on carbon grids from Ted Pella, Inc. Oxaliplatin Injection USP (Hospira, Inc.) was graciously donated by UCSD Moores Cancer Center (3855 Health Sciences Drive, La Jolla, CA). Tumors grown from HT-1080 fibrosarcoma cells (ATCC) were used for the model system, as this cell line overexpress MMPs (Yoon *et al.*, *J Biol Chem* **2001**, *276*, 20085). Nu/nu mice were obtained through the UCSD in-house breeding colony. Animals were inoculated with ~10^6 cells as a subcutaneous bolus, and treatments began once tumor mass reached ~50 mm^3. Animals were sacrificed at 12 days post-treatment. Calipers were used to record tumor volume daily over the course of the study. Absolute tumor volume was approximated with the formula: (1) V = 0.5 *length (mm) x $width^2$ (mm). Relative tumor volume was determined by the formula: (2) $V_{relative} = (V/V_i) * 100$, where V is the absolute tumor volume on the day of measurement

and V_i is the absolute tumor volume on the first day of treatment. Live-animal imaging was taken on a GE Art Optix instrument. For optical imaging, animals were anesthetized with isofluorane with an induction dose of 3% and a maintenance dose of 1.5% in an oxygen gas stream. After injection, animals were imaged at given timepoints using a GE ART eXplore Optix Instrument (λ_{ex}= 635 nm and λ_{em}= 693 nm). After sacrifice, tumors were harvested and frozen for tissue section preparation and analysis. Tumors were removed and frozen using cryoprotection and Optimum Cutting Temperature (O.C.T.) formulation. The tissue was then sectioned with a cryostat at 5 µm thickness and places on an ITO coverslip. A Zeiss ELYRA super resolution microscope located within the Environmental Molecular Sciences Laboratory at PNNL in Richland, WA was used for SIM imaging. A NanoSIMS 50L (Cameca, France) located within the Environmental Molecular Sciences Laboratory at PNNL in Richland, WA was used for secondary ion mass spectrometry imaging.

Safety Considerations

Standard laboratory safety protocols were followed in the performance of all procedures described herein. No unexpected hazards were encountered.

Polymer Synthesis

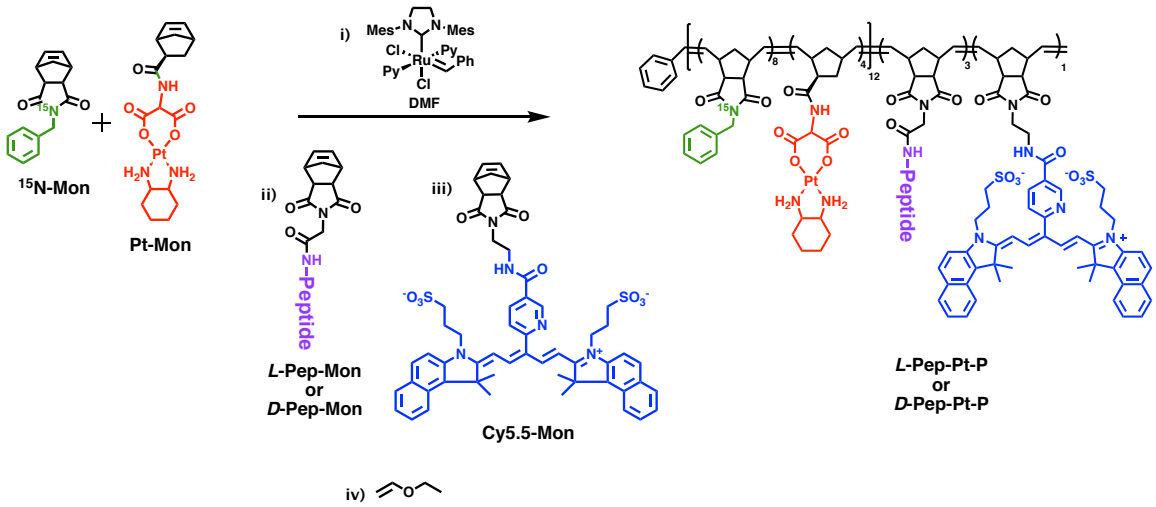

Figure S1. Synthetic route of multilabeled polymers ***L*-Pep-Pt-P** and ***D*-Pep-Pt-P**.

To a stirred solution of **^{15}N-Mon** (6.59 mg, 2.6 x10^{-5} mol, 8.4 equiv) in dry DMF (140 µL) was added a solution of the catalyst ($(IMesH_2)(C_5H_5N_2)(Cl)_2Ru$=CHPh) (2.36 mg, 3.2x$10^{-6}$ mol, 1.05 equiv) in dry DMF (105 µL) and a solution of **Pt-Mon** (7.08 mg, 1.3x10^{-5} mol, 4.2 equiv) in dry DMF (1700 µL). The reaction was allowed to stir under N_2 for 2 hours, after which an aliquot (30 µL) was removed and quenched with ethyl vinyl ether for Static Light Scattering (SLS) analysis. The remaining solution of **^{15}N-Mon** + **Pt-Mon** + catalyst (1800 µL) was split into two separate reaction

vessels. To one reaction vessel was added a solution of ***L*-Pep-Mon** (6.02 mg, $4.6x10^{-6}$ mol, 3 equiv) in 200 µL dry DMF (to ultimately afford ***L*-Pep-Pt-P**). To the second vessel was added a solution of ***D*-Pep-Mon** (6.02 mg, $4.6x10^{-6}$ mol, 3 equiv) in 200 µL dry DMF (to ultimately afford ***D*-Pep-Pt-P**). After three additional hours, a small aliquot was removed from each reaction vessel (30 µL each) and terminated with ethyl vinyl ether for SLS analysis. Then, to each of the polymer solutions was added **Cy-Mon** (1.16 mg, $1.2x10^{-6}$ mol, 0.75 equiv) and was allowed to stir for an additional two hours, before fully quenching the polymer solutions with ethyl vinyl ether. The fully terminated polymers were precipitated with a cold 1:1 ether:methanol solution to afford the block copolymers as dark yellow solids (***L*-Pep-Pt-P**, ***D*-Pep-Pt-P**).

Polymer Analysis by SLS:

		Mn	Mw	Dispersity
***L*-Pep-Pt-NP**	Block 1	6726	6856	1.019
	Full Polymer	8540	8980	1.051
	Block 2	1814	2124	--
***D*-Pep-Pt-NP**	Block 1	10870	11630	1.069
	Full Polymer	16010	17420	1.089
	Block 2	5140	5790	--

Nanoparticle Preparation and Characterization (*L*-Pep-Pt-NP and *D*-Pep-Pt-NP)

Polymers (***L*-Pep-Pt-P** or ***D*-Pep-Pt-P**) were was dissolved in DMSO at a concentration of 1.0 mg/mL with respect to polymer, and an additional 1 mL of 1X DPBS (Dulbecco's Phosphate Buffered Saline, no Ca, no Mg) was added over the course of 2 hours. These solutions were transferred to 3500 MWCO snakeskin dialysis tubing, and dialyzed against 1 L of 1X DPBS at pH 7.4 over 2 days with 2 buffer changes. The resulting solution was analyzed by DLS and TEM. (**See Figure S2 and S3**).

In Vitro Nanoparticle Degradation via MMP-12

500 µM ***L*-Pep-Pt-NP** (concentration with respect to peptide) or ***D*-Pep-Pt-NP** were incubated with MMP-12 (100 nU) at 37 degrees Celsius. After 24 hours, samples were analyzed via RP-HPLC (λ = 254 nm) to monitor for the presence of peptide cleavage fragments, with sequence LAGGERDG. Samples were also analyzed by DLS and negative stain TEM to monitor for aggregation following MMP cleavage. This aggregation event only occurs in the ***L*-Pep-Pt-NP** system, as evidenced by TEM and DLS. (See **Figure S2 and S3**).

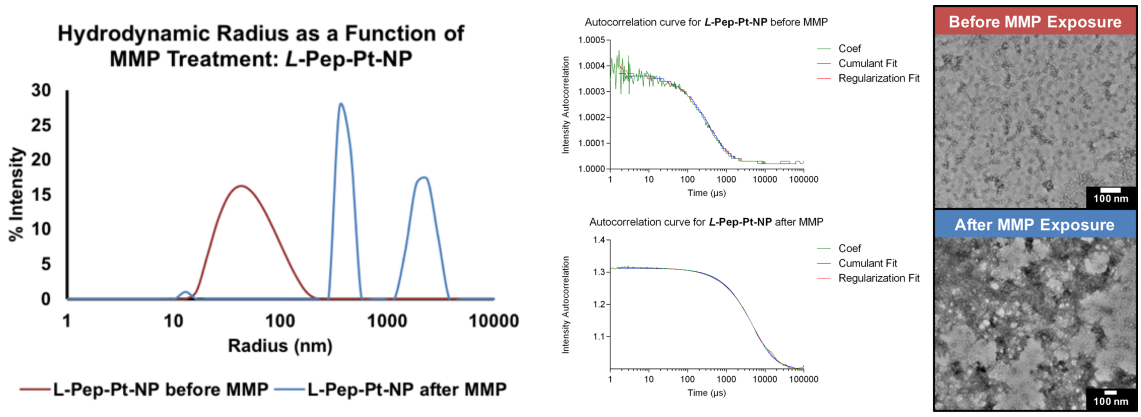

Figure S2. Nanoparticle size analysis of ***L*-Pep-Pt-NP** by DLS and TEM before (red) and after (blue) exposure to MMP-12. A drastic shift in hydrodynamic radius (DLS) and morphology (TEM) is observed.

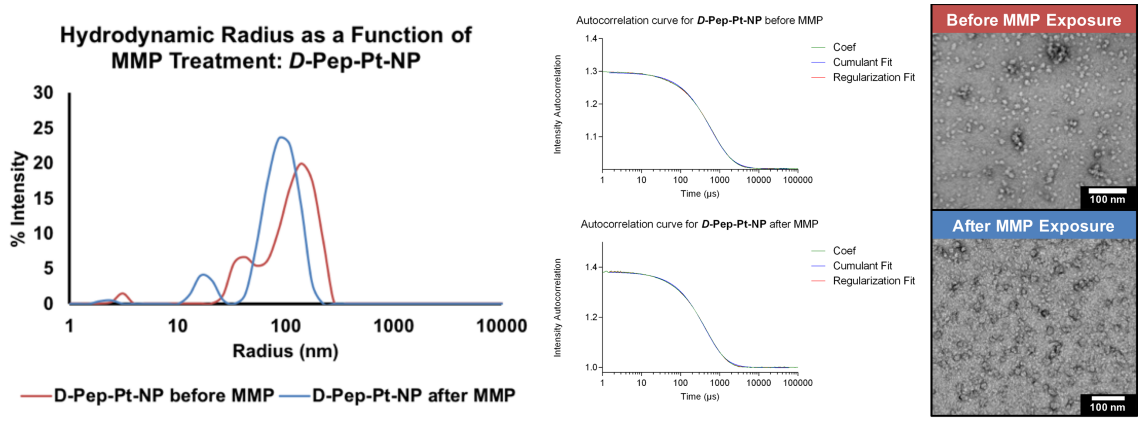

Figure S3. Nanoparticle size analysis of ***D*-Pep-Pt-NP** by DLS and TEM before (red) and after (blue) exposure to MMP-12. No appreciable difference in hydrodynamic radius (DLS) nor morphology (TEM) is observed.

Intratumoral Efficacy

16 tumor-bearing nu/nu female mice were randomly sorted into 4 groups (4 mice per cohort) and treated with ***L*-Pep-Pt-NP**, ***D*-Pep-Pt-NP**, oxaliplatin, or saline at the dosage equivalent of 2.5 mg/kg of Pt as a single intratumoral injection. Mouse weight and tumor volume were recorded once daily over the course of the 12-day study. Animals were imaged at 0, 4, 24, 48, and 72 hours post-injection via live-animal optical imaging (see **Figure 2** and **Figure S4**). To assess efficacy, relative tumor volume (see equation (1) above) was calculated for each data point. The average relative tumor volume of each cohort at each time point was then calculated, along with standard deviation and standard error of the mean. Animals were sacrificed at 12 days post-injection. For the *ex vivo* analysis, similar to the procedure used for efficacy studies, tumor-bearing mice were injected IT with either ***L*-Pep-Pt-NP**, ***D*-Pep-Pt-NP,** or saline solution and sacrificed 24 h later. Tumor, liver,

spleen, kidneys, heart, and lungs were excised from each animal and treated as in the above protocols.

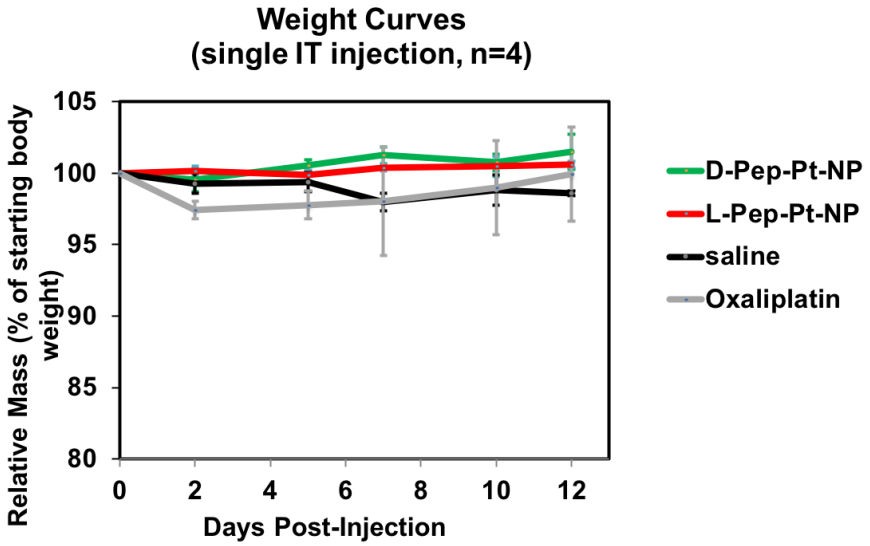

Figure S4. Mouse weight following IT injection of ***L*-Pep-Pt-NP** to ***D*-Pep-Pt-NP**, oxaliplatin at 2.5 mg/kg dose with respect to Pt and saline solution.

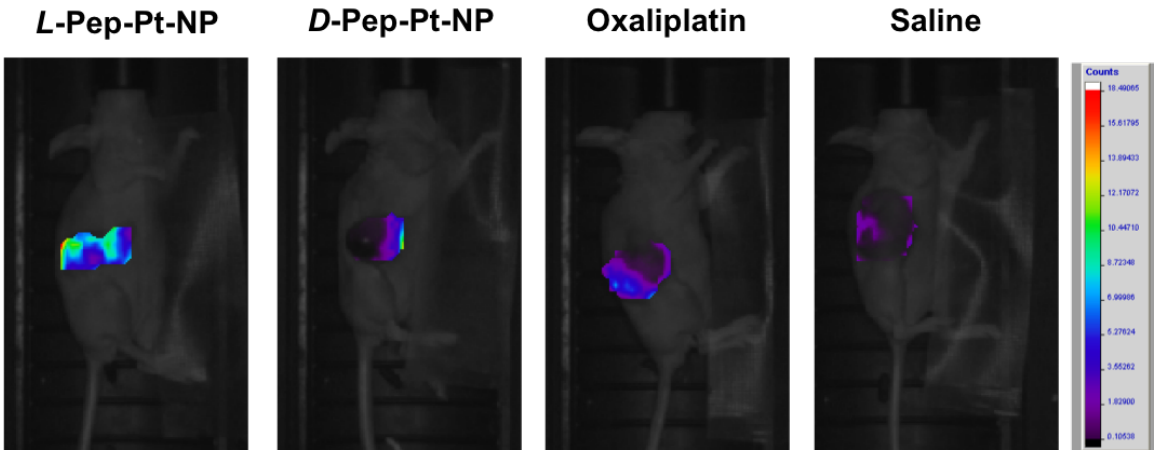

Figure S5. Live-animal fluorescence images after 5 days of IT injection of ***L*-Pep-Pt-NP**, ***D*-Pep-Pt-NP**, oxaliplatin and saline solution. Fluorescence signal rapidly diminishes post-injection in ***D*-Pep-Pt-NPs**, while the signal is still observed after 5 days for the ***L*-Pep-Pt-NPs**.

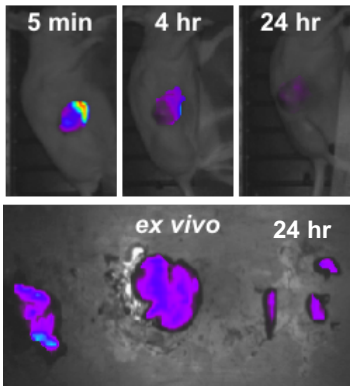

Figure S6. Live-animal (top) and *ex vivo* (bottom) images of animal administered ***D*-Pep-Pt-NP**. Fluorescence signal rapidly diminishes post-injection with little accumulation seen in organs at sacrifice 24 h after injection (bottom organs, left to right: tumor, liver, spleen, kidneys).

Fluorescent IHC Staining of Tissue Sections

Tissue sections on 18 mm^2 ITO coverslips (70-100 Ω, 6462-AB, SPI supplies) were fixed for 10 min with acetone at room temperature and washed three times with PBSt (0.05% Tween in PBS). Sections were incubated with blocking solution (1% BSA in PBSt) for 15 min. The primary antibody mouse anti-α-actinin (A7811, Sigma Aldrich) was added in a 1/200 dilution in blocking buffer and incubated at 4 °C overnight. Tissues were washed three times with PBSt and the secondary antibody goat anti-mouse AlexaFluor 488 (A11001, Life Technologies) was added in a 1/400 dilution in blocking buffer and incubated for 30 min. Tissue sections were washed three times with PBSt and were incubated for 10 min with a 300 nM solution of DAPI. The tissue sections were finally washed three times with PBSt and then subjected to a series of dehydration washes with 30%, 50%, 70%, 80% ethanol solutions and 3 times with 100% ethanol (30 min each).

Fluorescence Imaging by Wide-field and Structural Illumination Microscopy (SIM)

SIM and wide-field fluorescence imaging was performed on the Elyra S1 inverted fluorescence microscope (Zeiss). To survey a large area of a tissue section, wide-field fluorescence microscopy with a 10X magnification objective was used. Multiple images were tiled to cover a large area. SIM was used to obtain high magnification, high resolution images, an oil immersion objective with 100X magnification and 1.4 numerical aperture was used in this study. The same set of lasers and fluorescence filters were used for wide-field fluorescence and SIM imaging. For every sample, 3 tracks were recorded sequentially to: (1) image the NPs (Cy5.5) using 642 nm laser excitation with emission wavelength longer than 655 nm; (2) image the cellular bodies (α-actinin) using 488 nm laser excitation with emission band 495 nm to 550 nm; and (3) image the nucleus (DAPI) using 405 nm laser excitation with emission band 420 nm to 480 nm. The laser power was adjusted

accordingly due to the difference in signal level from different objectives. 3 rotations and 5 phases were taken for each SIM image. The resolution in the raw images was 80 nm per pixel, and in the resulting super resolution images was 40 nm per pixel. The camera exposure time was 100 ms per image. In SIM, the multi-phase/rotation/track data were later processed to obtain super resolution images using the ZEN software (Zeiss).

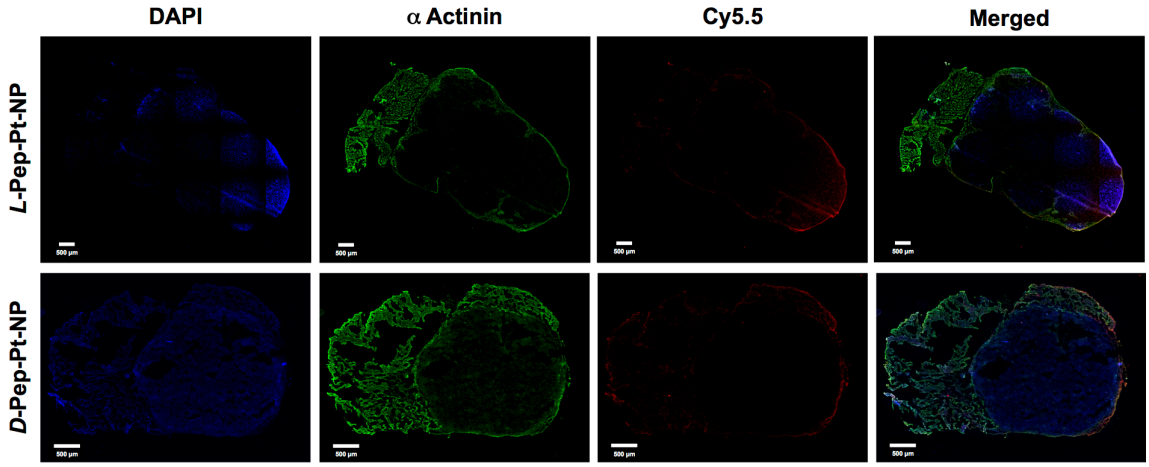

Figure S7. 10X magnification fluorescence image of tumor sections from mice treated with ***L*-Pep-Pt-NP** (top) and ***D*-Pep-Pt-NP** (bottom). In both cases the signal of the nanoparticles (Cy5.5) is concentrated on the periphery of the sections.

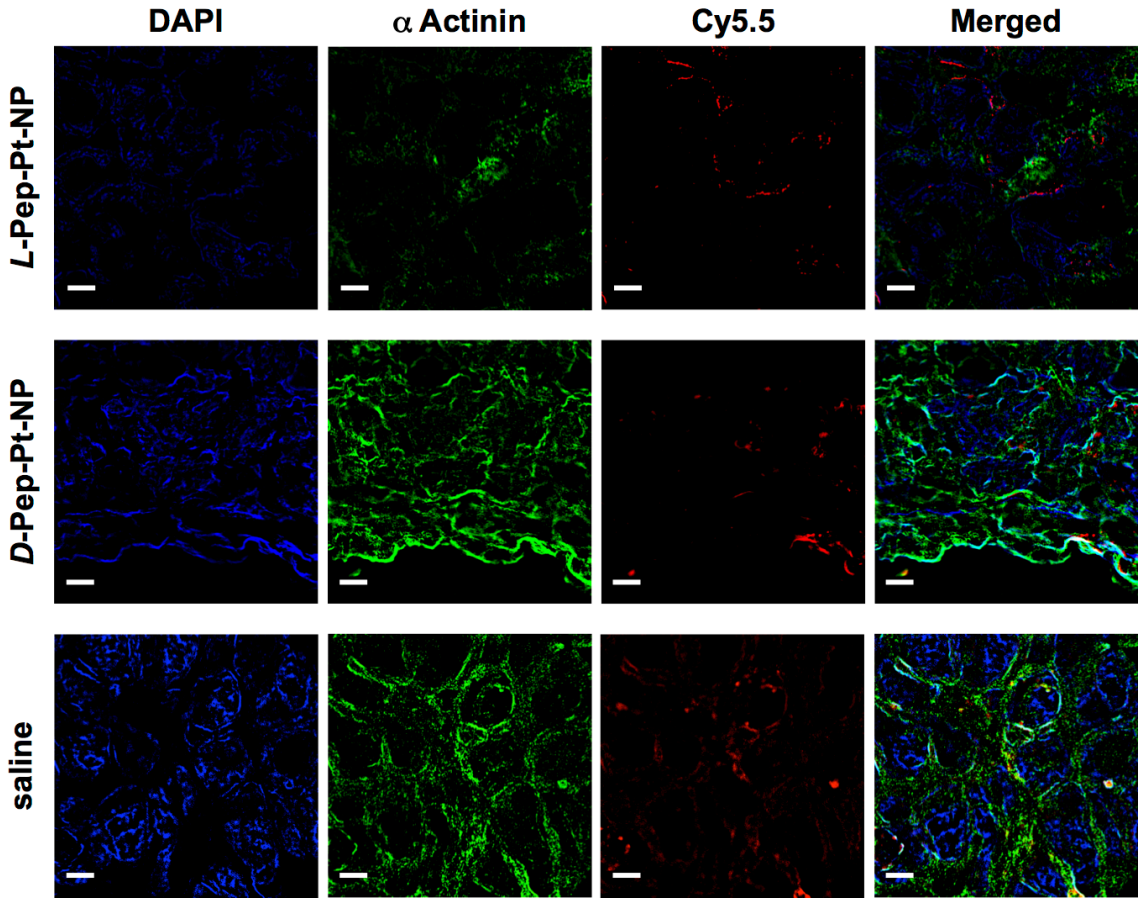

Figure S8. 100X magnification SIM images of tumor sections from mice treated with ***L*-Pep-Pt-NP** (top), ***D*-Pep-Pt-NP** (middle) and saline solution (bottom). Scale bars represent 5 μm.

NanoSIMS Imaging

For NanoSIMS analyses, the samples were coated with 10 nm of Au prior to analysis to minimize sample charging. Samples were presputtered with about 2 × 10^{16} ions cm^{-2} after which, images sized 48 μm × 48 μm containing 256 pixel × 256 pixel were acquired with a 16 keV, ~1.5 pA Cs^+ primary ion beam (width ~115 nm) using magnetic peak switching, where in the first two planes $^{12}C^{14}N^-$, $^{31}P^-$ and $^{195}Pt^-$ were collected (13.5 ms/pixel). After the first two planes, the detector collecting $^{12}C^{14}N^-$ was moved to collect $^{12}C^{15}N^-$ and in the second scan of the plane $^{12}C^{15}N^-$, $^{31}P^-$ and $^{195}Pt^-$ were collected in two consecutive planes at 13.5 ms/pixel). Secondary electron images (SE) were also collected for all analyses. Data was processed using OpenMIMS (National Resource for Imaging Mass Spectrometry, Harvard University, Cambridge), which is an ImageJ plugin (U. S. National Institutes of Health, Bethesda, Maryland) in which pixel by pixel deadtime (44 ns) and QSA (β = 0.5) corrections were applied. Data from ROIs were further processed in a spreadsheet. Prior to tumor analyses, yeast standards with known $\delta^{15}N$ (+0.35, personal communication Jim Moran PNNL) were imaged each day with identical analysis conditions to those

used with the tumor sections. 16 ROIs were drawn around the yeast and used to correct each day's data. There appeared to be a minor interference associated with ^{195}Pt as evidenced in a small background, however Pt-treated cells had hotspots with significantly higher intensity than background.

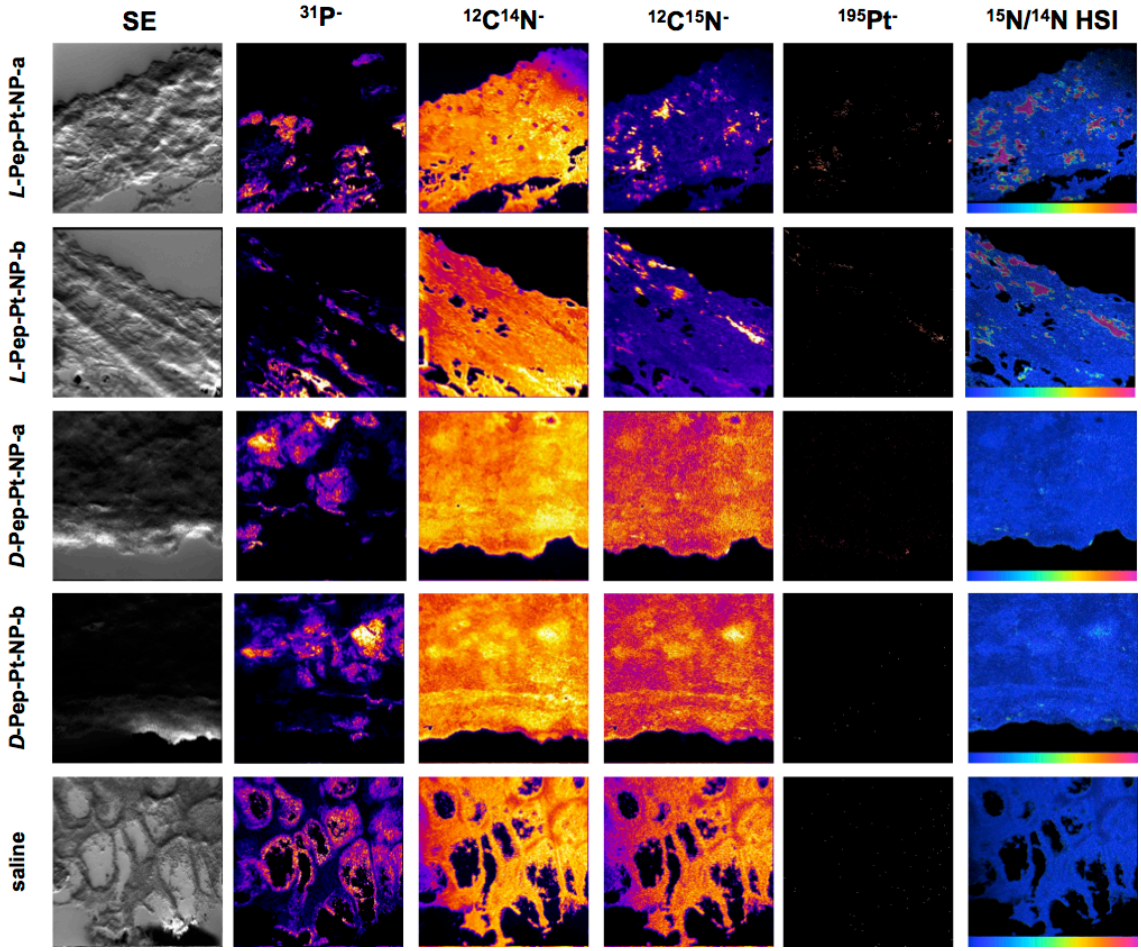

Figure S9. NanoSIMS images of tumor sections from mice treated with ***L*-Pep-Pt-NP**, ***D*-Pep-Pt-NP** and saline solution. The scales on the HSI images were set up for each case in particular to highlight the features of the image: ***D*-Pep-Pt-NP-a** .0037 to .015, ***D*-Pep-Pt-NP-b** .0037 to .014, ***L*-Pep-Pt-NP-a** 0.0037 to 0.012, ***L*-Pep-Pt-NP-b** 0.0037 to 0.012 and saline 0.0037 to 0.015.

SIM and NanoSIMS Correlated Images

NanoSIMS images were transformed using Matlab software to correlate with SIM images acquired on similar areas. Thus, all three signals observed on SIM images can be correlated with the seven acquired NanoSIMS images representing different ion maps.

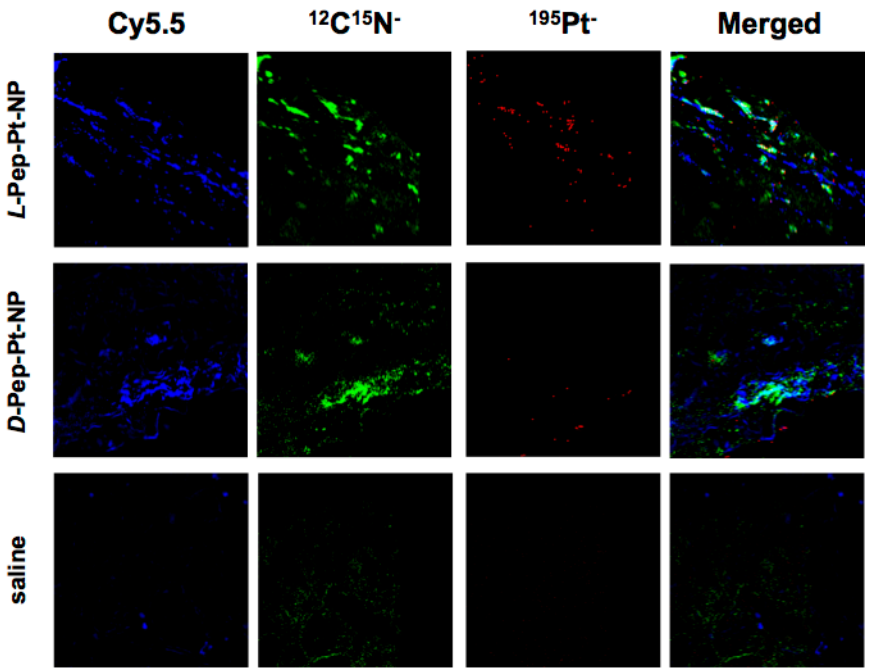

Figure S10. Overlay between the 3 different labels introduced in the polymers. Cy5.5 in blue (nanocarrier), $^{12}C^{15}N^-$ in green (nanocarrier) and $^{195}Pt^-$ in red (Pt-drug). The correlation was carried out for images from the three different studied conditions: tumor sections from mice treated with ***L*-Pep-Pt-NP** (top), ***D*-Pep-Pt-NP** (middle) and saline solution (bottom). While Cy5.5 and $^{12}C^{15}N^-$ images show large areas of overlap for ***L*-Pep-Pt-NP** and ***D*-Pep-Pt-NP**, $^{195}Pt^-$ shows hotspots which correlate only partially. As expected, saline samples show only low signal (Cy5.5) or counts for $^{12}C^{15}N^-$ and $^{195}Pt^-$.

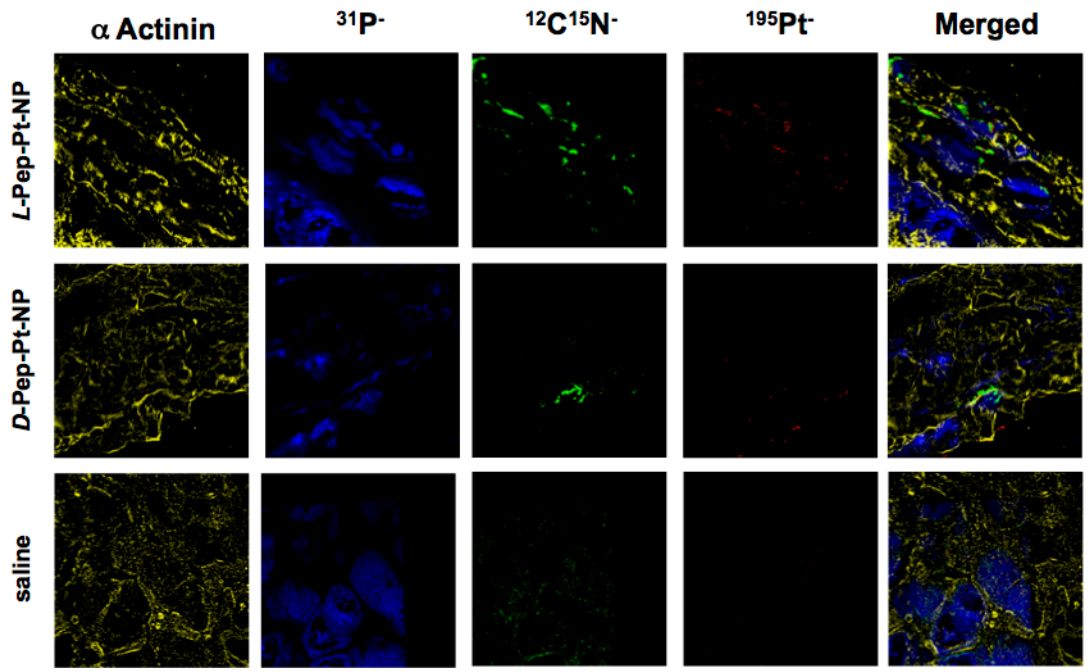

Figure S11. As another example of SIM and NanoSIMS correlation, shown in this figure is the overlay of the fluorescent images prestained for α-actinin (cellular bodies, yellow), with $^{31}P^-$ ion map (nucleus, blue), $^{12}C^{15}N^-$ (nanocarrier, green) and $^{195}Pt^-$ (Pt-drug, red). The correlation was carried out for images from the three different studied conditions: tumor sections from mice treated with ***L*-Pep-Pt-NP** (top), ***D*-Pep-Pt-NP** (middle) and saline solution (bottom).

Statistical Analysis of NanoSIMS Data

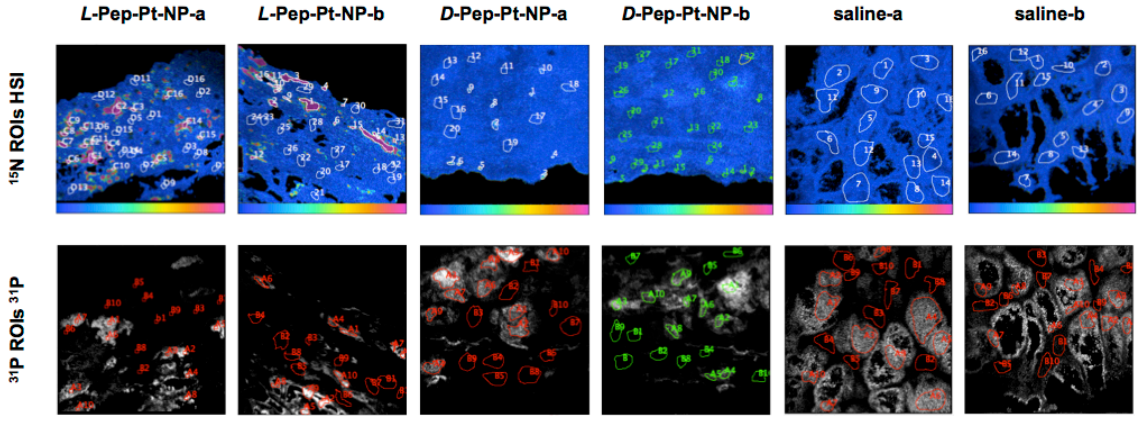

Figure S12. NanoSIMS images of tumor sections from mice treated with ***L*-Pep-Pt-NP**, ***D*-Pep-Pt-NP,** or saline solution. In ***L*-Pep-Pt-NP** and ***D*-Pep-Pt-NP** HSI images, 16 ROIs were selected inside of ^{15}N hotspots and 16 ROIs outside of ^{15}N hotspots. In saline HSI images, 16 ROIs were selected on ^{15}N containing areas, since no ^{15}N hotspots were observed. In $^{31}P^-$ images, 10 ROIs were selected inside of ^{31}P hotspots and 10 ROIs outside of ^{31}P hotspots.

The first step for NanoSIMS data processing involved correcting the counts obtained for ^{15}N and ^{14}N against the standard yeast sample, which was measured each day before any of the tumor samples. Thus, this yeast standard was used to correct the $^{15}N/^{14}N$ ratio relative to air, $\delta^{15}N \sim 0.35‰$ (Jim Moran, personal communication). Those were called "corrected $^{15}N/^{14}N$ values" and were used for all further calculations.

Note that Pt^- was collected as ^{196}Pt for the saline sample. Pt counts on saline ROIs were normalized to ^{195}Pt by multiplying by 1.34, according to their isotopic abundance (33.8/25.2).

Inside/outside of ^{15}N-rich ROIs: For samples containing **Pep-Pt-NP**, 16/16 ROIs inside/outside of ^{15}N-rich areas were selected from 3 independent images. On the saline sample, 16 ROIs were selected on tissue from 2 different images. Each ROI value was obtained as the average counts per pixel in the ROI.

Inside/outside of ^{31}P-rich ROIs: 10/10 ROIs inside/outside of ^{31}P-rich areas were selected from 3 independent images for the samples containing **Pep-Pt-NP** and from 2 independent images for the saline samples.

ROI counts (as a ratio counts/area) were averaged for the different groups, leaving out the average of those considered as outliers (values higher or lower to IQR*1.5).

Those averages and corresponding SE are listed in Table S1 and Table S2.

Additional statistical analyses were performed with Graphpad software with these values to compare bars on graphs of Figure 5 in the main text. The results of unpaired *t* tests are shown in Table S3.

Table S1. $^{15}N/^{14}N$ and ^{195}Pt counts for ROIs of selected inside and outside of ^{15}N-rich areas. Values are means ± 1 SE

	***L*-Pep-Pt-NP**	***D*-Pep-Pt-NP**	Saline
$^{15}N/^{14}N$ inside	0.02966 ± 0.00132	0.00597 ± 0.00021	0.00346 ± 0.00002
$^{15}N/^{14}N$ outside	0.00499 ± 0.00002	0.00369 ± 0.00002	
^{195}Pt inside	0.3480 ± 0.0339	0.0882 ± 0.0114	0.0030 ± 0.0005
^{195}Pt outside	0.0080 ± 0.0012	0.0057 ± 0.0010	

Table S2. $^{15}N/^{14}N$ and ^{195}Pt counts for ROIs selected inside and outside of ^{31}P-rich areas. Values are means ± 1 SE

	***L*-Pep-Pt-NP**	***D*-Pep-Pt-NP**	Saline
$^{15}N/^{14}N$ inside	0.00450 ± 0.00019	0.00373 ± 0.00004	0.00343 ± 0.00003
$^{15}N/^{14}N$ outside	0.00407 ± 0.00003	0.00369 ± 0.00003	
^{195}Pt inside	0.0365 ± 0.0056	0.0147 ± 0.0017	0.0023 ± 0.0004
^{195}Pt outside	0.0147 ± 0.0026	0.0065 ± 0.0011	

Table S3. Statistical analysis for graphs on Figure 5 of the main text

Graph A.3: $^{15}N/^{14}N$ inside and outside of ^{15}N-rich ROIs		
Variables analyzed	***p* value**	**Significance**
L-Pep-Pt-NP inside *vs. L*-Pep-Pt-NP outside	$p \leq 0.0001$	****
D-Pep-Pt-NP inside *vs. D*-Pep-Pt-NP outside	$p \leq 0.0001$	****
L-Pep-Pt-NP inside *vs. D*-Pep-Pt-NP inside	$p \leq 0.0001$	****
L-Pep-Pt-NP outside *vs. D*-Pep-Pt-NP outside	$p \leq 0.0001$	****
L-Pep-Pt-NP outside *vs.* saline	$p \leq 0.0001$	****
D-Pep-Pt-NP outside *vs.* saline	$p \leq 0.0001$	****
Graph A.4: ^{195}Pt inside and outside of ^{15}N-rich ROIs		
Variables analyzed	***p* value**	**Significance**
L-Pep-Pt-NP inside *vs. L*-Pep-Pt-NP outside	$p \leq 0.0001$	****
D-Pep-Pt-NP inside *vs. D*-Pep-Pt-NP outside	$p \leq 0.0001$	****
L-Pep-Pt-NP inside *vs. D*-Pep-Pt-NP inside	$p \leq 0.0001$	****
L-Pep-Pt-NP outside *vs. D*-Pep-Pt-NP outside	0.1739	ns
L-Pep-Pt-NP outside *vs.* saline	0.0086	**
D-Pep-Pt-NP outside *vs.* saline	0.3702	ns
Graph B.3: $^{15}N/^{14}N$ inside and outside of ^{31}P-rich ROIs		
Variables analyzed	***p* value**	**Significance**
L-Pep-Pt-NP inside *vs. L*-Pep-Pt-NP outside	0.1392	ns
D-Pep-Pt-NP inside *vs. D*-Pep-Pt-NP outside	0.5494	ns
L-Pep-Pt-NP inside *vs. D*-Pep-Pt-NP inside	$p \leq 0.0001$	****
L-Pep-Pt-NP outside *vs. D*-Pep-Pt-NP outside	$p \leq 0.0001$	****
L-Pep-Pt-NP outside *vs.* saline	$p \leq 0.0001$	****
D-Pep-Pt-NP outside *vs.* saline	$p \leq 0.0001$	****
Graph B.4: ^{195}Pt inside and outside of ^{31}P-rich ROIs		
Variables analyzed	***p* value**	**Significance**
L-Pep-Pt-NP inside *vs. L*-Pep-Pt-NP outside	0.0017	**
D-Pep-Pt-NP inside *vs. D*-Pep-Pt-NP outside	0.0002	***
L-Pep-Pt-NP inside *vs. D*-Pep-Pt-NP inside	0.0025	**

L-Pep-Pt-NP outside *vs. D*-Pep-Pt-NP outside	0.0279	*
L-Pep-Pt-NP outside *vs.* saline	$p \leq 0.0001$	****
D-Pep-Pt-NP outside *vs.* saline	0.0007	***